JOURNAL OF PROPULSION AND POWER
Vol. 24, No. 6, November–December 2008

# Thrust Stand Micromass Balance for the Direct Measurement of Specific Impulse

Andrew D. Ketsdever*
*University of Colorado at Colorado Springs, Colorado Springs, Colorado 80933*
and
Brian C. D'Souza† and Riki H. Lee†
*University of Southern California, Los Angeles, California 90089-1191*

DOI: 10.2514/1.36921

**A technique has been developed to directly measure the specific impulse from pulsed thruster systems. The technique is especially useful for propulsion devices that use solid propellants, for which a direct measurement of the propellant mass flow is extremely difficult. A torsion balance is used with a horizontal axis of rotation. A thruster is placed on the balance such that the impulse of the thruster firing and the change in mass due to the expelled propellant act in the same direction. A combined impulse and steady-state force measurement (due to propellant mass loss) can then be decoupled to assess the ratio of the impulse to the weight of propellant expended, or the specific impulse. A model has been developed to show the utility of the technique for pulsed systems with a firing time less than the natural period of the balance. An experimental proof of principle study was also undertaken using the laser ablation of engineering-grade Buna, Viton, and Teflon propellants. Specific-impulse measurements on the order of 200 s have been demonstrated with this laser ablation thruster.**

## Nomenclature

| | | |
|---|---|---|
| $C$ | = | torsional damping coefficient, N · m s/rad |
| $C_m$ | = | laser-material momentum coupling coefficient, dyne/W |
| $E$ | = | laser energy, W |
| $F_C$ | = | static calibration force, N |
| $g_o$ | = | acceleration due to gravity on Earth, m/s$^2$ |
| $I$ | = | mass moment of inertia, N · m s$^2$/rad, kg · m$^2$/rad |
| $I_{sp}$ | = | specific impulse, s |
| $I_{tot}$ | = | total impulse, N · s |
| $K$ | = | torsional spring constant, N · m/rad |
| $M$ | = | forcing moment, N · m |
| $M_o$ | = | steady-state forcing moment, N · m |
| $P$ | = | laser power, J |
| $Q^*$ | = | laser energy consumed per unit mass ablated, J/kg |
| $R_C$ | = | radial distance from pivot to center of calibration load, m |
| $R_L$ | = | radial distance from pivot to linear variable differential transformer, m |
| $R_R$ | = | radial distance from pivot to center of test load, m |
| $T$ | = | natural period of the stand, s |
| $t$ | = | time, s |
| $X$ | = | measured linear variable differential transformer deflection, m |
| $\Delta m$ | = | change in mass due to laser ablation, kg |
| $\delta_n$ | = | logarithmic decrement |
| $\zeta$ | = | damping ratio |
| $\theta$ | = | angular deflection, rad |
| $\tau$ | = | pulse duration, s |
| $\omega_o$ | = | natural frequency, rad/s |
| $\omega_d$ | = | damped frequency, rad/s |

Presented as Paper 5300 at the 43rd AIAA/ASME/SAE/ASEE Joint Propulsion Conference and Exhibit, Cincinnati, OH, 8–11 July 2007; received 30 January 2008; accepted for publication 13 May 2008. 

*Group Leader, Aerophysics Branch, Department of Mechanical and Aerospace Engineering. Senior Member AIAA.

†Graduate Research Assistant, Department of Aerospace and Mechanical Engineering. Student Member AIAA.

## Introduction

THE impulse produced by a thruster can be found by integrating the thrust produced with time. The specific impulse $I_{sp}$ is defined as the impulse delivered by a propulsion system divided by the weight of the propellant used to produce that impulse [1]. Traditional specific-impulse measurements for propulsion systems that use solid propellants are complicated by several issues. First, the amount of mass loss and the associated impulse provided by pulsed systems may be relatively low, requiring the averaging of multiple thruster firings to obtain meaningful data. The performance of individual pulses can be lost through the averaging of multiple tests. Understanding of individual pulse performance can lead to more efficient thrusters if parameters between subsequent tests can be quantified.

Second, the system mass is traditionally measured before the performance measurements, and again after, to assess the propellant mass used [2]. These measurements may take place days apart and may require the system to be placed into a vacuum chamber and subsequently removed between thruster firings at the cost of valuable resources. Finally, issues of handling, contamination, oxidation, and adsorption may complicate mass measurements that are not done in situ.

To combat these issues for pulsed thruster systems, a thrust stand mass balance (TSMB) and associated experimental techniques have been developed in which both the total mass loss and impulse are measured simultaneously. The concurrent measurement of the impulse and mass loss leads to a direct measure of specific impulse. The benefits of the developed technique include the ability to measure specific impulse directly and in situ without the complications and potential inaccuracies of multiple measurements. The resolution of the TSMB is such that it could measure the impulse and mass loss of individual pulses from most micropropulsion systems currently under development. The developed technique allows both mass and impulse measurements simultaneously while the thruster is in vacuum, reducing the influence of oxidation, adsorption, and contamination. The major limitation of the technique is that it is only currently valid for pulsed systems in which the pulse width is less than the natural period of the thrust stand.

The technique has been applied in this work to investigate a laser ablation system, although the technique is also valid for a variety of pulsed propulsion systems such as solid microthrusters [3] and pulsed plasma thrusters [4]. Laser ablation affords some benefits

when developing the TSMB. First, the laser pulse energy can be tuned to allow more or less ablative mass loss in a particular laser pulse. Second, a variety of propellants (target materials) can be used to assess the ability of the technique to distinguish the specific impulse over a relatively wide range. One of the disadvantages to using laser propulsion is the inherent scatter in the data between pulses. Drift in the laser energy output and physical differences between ablation sites on engineering targets account for much of the scatter. However, this scatter can also be viewed as a benefit in the development of the TSMB because the ability to measure the performance of individual impulses can be demonstrated.

Numerous experimental techniques have been employed in the past to measure mass loss and other fundamental properties of laser ablation events. The techniques include time-of-flight mass spectroscopy, plasma spectroscopy, nanosecond-shadowgraphy [5], and other plasma imaging techniques [6]. Each technique may be useful in understanding certain aspects as they monitor specific components of the ejected material. However, each has limitations and weaknesses in their application for investigating a broad range of mechanisms for laser ablation. Because the ejected material is expected to contain particles of different sizes, charged and neutrals particles, and particles of varying velocity, it is difficult to simultaneously capture all components to accurately determine the amount of mass lost. By only monitoring some portions of the ablated material, it is often possible to underestimate the mass loss, which generally results in overestimating the specific impulse.

## Thrust Stand Mass Balance

The TSMB is based on the nano-Newton-second impulse balance system (NIBS) described by D'Souza and Ketsdever [7]. By inverting the NIBS to allow for a horizontal axis of rotation, both the impulse and the change in mass from the propulsive event provide forces acting in the same direction, as illustrated in Fig. 1. In this system, the weight of the propulsion system acts as a steady-state force on the TSMB. As a thruster fires, mass is released and the propulsion system gets lighter, with the change in mass resulting in a measurable deflection of the TSMB. The resulting steady deflection is calibrated to indicate the net change in mass due to the loss of propellant. With both the impulse and mass loss force acting in the same direction, the two forces couple to produce a single deflection trace on the TSMB. For the performance of the thruster to be quantified, each component must be resolved individually from the single deflection trace.

To assess the feasibility of such an analysis, a model was created to simulate the behavior of the TSMB. The TSMB model is based directly on the NIBS model [7]. The model takes the force profile for each component (impulse and weight change) and plots their individual and combined dynamic effects on the TSMB. The TSMB behaves like an underdamped, oscillating, mass-spring system. System motion is described by the following second-order differential equation for a rigid bar:

$$I\ddot{\theta}(t) + C\dot{\theta}(t) + K\theta(t) = M(t) = F(t)r \tag{1}$$

For small angles of deflection $\theta$, the motion of the stand can be linearly approximated through the small-angle approximation, such that Eq. (1) can be written as

$$I\frac{\ddot{X}(t)}{R_L} + C\frac{\dot{X}(t)}{R_L} + K\frac{X(t)}{R_L} = F(t)R_R \tag{2}$$

To derive the forcing function from a measured deflection, the coefficients in Eq. (2) must be experimentally measured from the TSMB. By applying a steady-state calibration force to the stand, the resulting deflection, as time goes to infinity, becomes

$$K\frac{X}{R_L} = F_C R_C \tag{3}$$

The remaining two coefficients can be found by analyzing the measured period and the decay of the deflection amplitude as a function of time. First, a logarithmic decrement is defined as

$$\delta_n = \ell_n(X_i/X_{i+n}) \tag{4}$$

where $i$ is a positive integer, and $X_i$ and $X_{i+n}$ are peak amplitudes, separated by $n$ periods. The damping ratio is then given by

$$\zeta = \delta_n/\sqrt{(n\cdot 2\pi)^2 + \delta_n^2} \tag{5}$$

The measured frequency of the stand can be found from the measured period and related to the natural frequency by

$$\frac{2\pi}{T} = \omega_d = \omega_o\sqrt{1-\zeta^2} \tag{6}$$

and the mass moment of inertia and damping coefficients are

$$I = \frac{K}{\omega_o^2} \tag{7}$$

$$C = 2\zeta\sqrt{KI} \tag{8}$$

Therefore, the coefficients $I$, $C$, and $K$ may be determined from any single test trace resulting from a known, static, steady-state, calibration load. It follows that if the deflection $X(t)$, resulting from a dynamic load, is measured on a stand with no significant change in $I$, $C$, or $K$, the time dependent function $F(t)$, which describes that dynamic load, may be determined through Eq. (2). Therefore, the system in Eq. (1) can be solved numerically for a steady-state forcing function as

$$\theta(t) = \frac{M_o}{K} + e^{\alpha t}\left[\left(\theta_o - \frac{M_o}{K}\right)\cos(\beta t) + \left(\frac{\dot{\theta}_o K - \alpha K\theta_o + \alpha M_o}{K\beta}\right)\sin(\beta t)\right] \tag{9}$$

$$\dot{\theta}(t) = e^{\alpha t}\left[\dot{\theta}_o\cos(\beta t) + \left(\frac{I\alpha\dot{\theta}_o - K\theta_o + M_o}{I\beta}\right)\sin(\beta t)\right] \tag{10}$$

$$\ddot{\theta}(t) = e^{\alpha t}\left[\left(\frac{M_o - C\dot{\theta}_o - K\theta_o}{I}\right)\cos(\beta t) + \left(\frac{\alpha(M_o - C\dot{\theta}_o - K\theta_o) - K\dot{\theta}_o}{I\beta}\right)\sin(\beta t)\right] \tag{11}$$

where $\alpha = -C/2I$ and $\beta = \sqrt{K/I - \alpha^2}$.

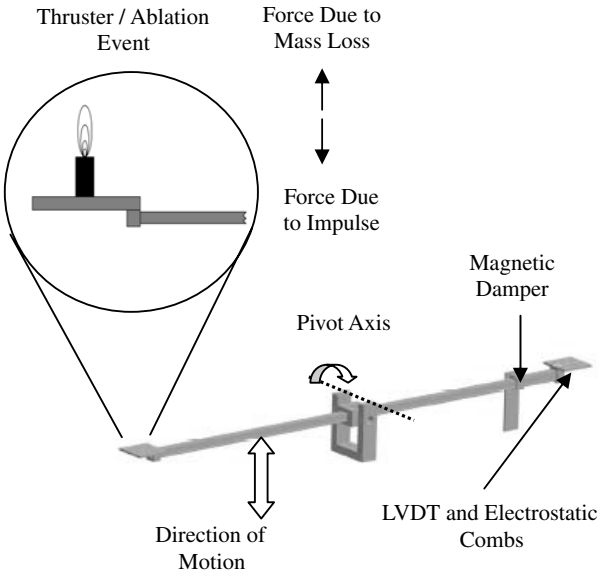


**Fig. 1 Schematic of the TSMB setup and configuration.**

It has already been shown that any arbitrary or irregular force can be approximated using a series of constant-force segments of small time widths $d\tau$ [7]. As such, the combined effect of two overlapping forces does not pose a particular problem for the TSMB. For simplicity, a constant force **F** is applied for a duration of $\tau$, resulting in the modeling of an impulse bit. The force profile corresponding to the mass change can be determined for a given specific impulse such that the weight loss is given by the total impulse ($\mathbf{F}^*\tau$) divided by the specific impulse. Assuming that the mass loss occurs steadily over the duration of the impulse, the force profile for the mass loss ramps up to a plateau, as seen in Fig. 2. Figure 2 shows the manifested force applied to the TSMB by the propellant mass loss and by the thruster impulse.

Figure 3 shows results from the TSMB model for a simulated pulsed thruster delivering a typical impulse of 1 mN · s. Shown are traces for the dynamic response of the TSMB for each effect individually and their combined result on the TSMB. The individual traces (for mass loss and impulse) assume that the TSMB has experienced only that force in the absence of the other. It is evident in Fig. 3 that between the individual impulse trace and mass loss trace, a phase shift exists in the timing, which results from the accommodation of the stand to the effective natural period of oscillation. In the case of the impulse, the pulse width is short relative to the natural period of the TSMB, allowing the stand to accommodate almost instantaneously. However, the force associated with the mass loss is continuously applied. This manifests as a slight phase shift in the two individual effect curves that, when combined, results in a curve that is close in magnitude to the curve for the impulse acting by itself but is temporally shifted. Because of the fact that the impulse is measured by taking the range of deflection from the first peak to the first valley, the magnitude of the curve for the impulse acting alone tends to be preserved in the combined trace. The mass loss is then simply measured by examining the total deflection of the tail of the trace compared with the initial zero point.

To verify that the magnitude of the impulse is preserved and can be decoupled from the mass loss, the input parameters of pulse width, specific impulse, and total impulse were varied in the model. The total impulses were varied from 3 nN · s up to 1 mN · s to fully cover the dynamic range of the stand, which was limited by the sensitivity of the current version of the TSMB. This entire impulse range was generated using a wide range of simulated pulse widths that were all less than the natural period of the stand, $T$. Additionally, for each set of impulse and pulse-width parameters, the specific impulse was varied from 1 to over 25,000 s. The results are summarized in Fig. 4 for an impulse of 1 mN · s. The spread in the data points (represented by error bars) shows the effects of the variation in specific impulse from 1 to 25,000 s. The magnitude of the mass loss varies with the specific impulse and has varying effects on the resulting TSMB deflection. It is interesting to note that the mass loss effect for a given impulse consistently manifests itself as a percentage of the impulse magnitude, such that smaller impulses result in proportionately smaller errors. For pulse widths below a tenth of the natural period, the deflection for a given specific impulse appears to be constant. For pulse widths above a tenth of a period, an expected decrease in the overall TSMB deflection is evident. Figure 4 also shows that as the pulse width approaches the natural period of the TSMB, the range of error from the mass loss increases, which results from the accommodation to the natural period. As the pulse width increases, the impulse component of the trace begins to shift in phase. Similar to the superposition of waves out of phase, constructive and destructive interference can be expected. As the phases between the components begin to synchronize, constructive interference results in larger error in the magnitude of the deflection range.

Figure 5 depicts the trend of the error caused by simultaneously measuring the impulse and the corresponding mass loss. Note that Fig. 5 only includes points for pulse widths less than 0.25 T, to

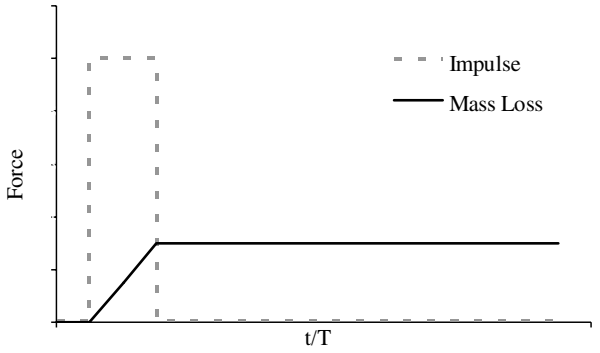


**Fig. 2 Force profiles for an impulse and its corresponding mass loss.**

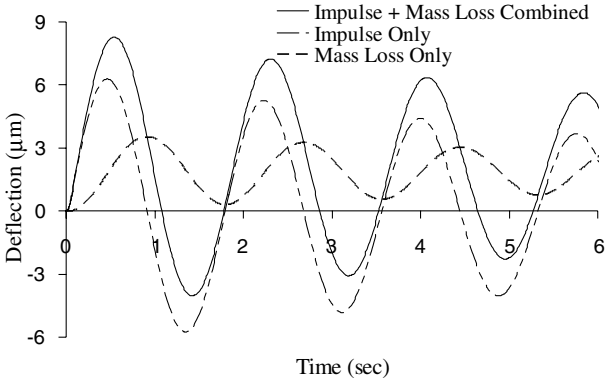


**Fig. 3 Individual impulse and mass loss traces generated by model simulation.**

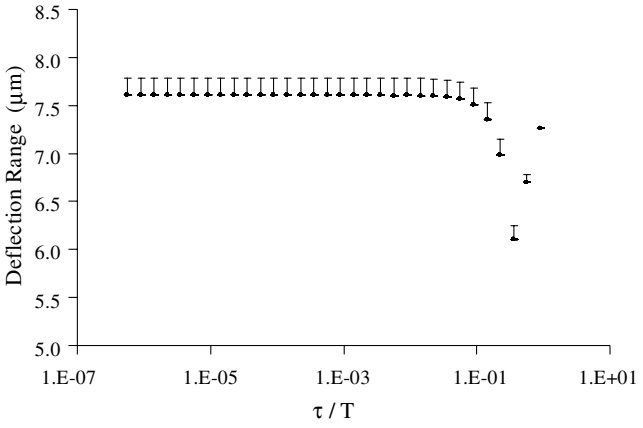


**Fig. 4 TSMB maximum deflection as a function of normalized impulse pulse width compared with the analytical model results.**

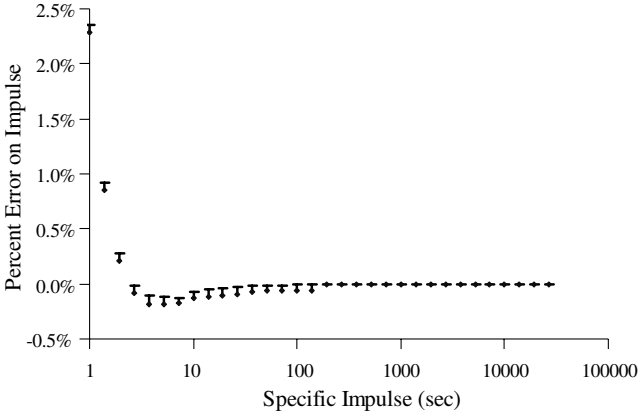


**Fig. 5 Error profile for impulse measurements with simultaneous mass loss measurements. This curve can be used to correct calculated impulses once the $I_{sp}$ of the thruster has been determined.**

minimize the scatter that is caused by pulse-width effects. Above a specific impulse of approximately 2 s, the percentage error in the calculated deflection range is less than 0.5%. For specific-impulse ranges in which thrusters would typically be tested, the error is almost negligible. Therefore, the standard and simple deflection technique for measuring impulse is sufficient for most micropropulsion systems currently being developed.

## Experimental Setup

The TSMB, shown in Fig. 1, is a torsion balance that consists of two flexure pivots that are used to support the balance and to provide a restoring force and is similar to the thrust stand described by Jamison et al. [8] The flexures have a spring constant of approximately 0.0016 Nm/ deg. The TSMB is completely symmetric about the center of rotation, with two armatures extending from each side of the stand. The TSMB is inertially balanced to reduce the effects of outside vibrations on the measurements. The force measurements involve the sensing of an angular displacement resulting from the torque applied to the damped rotary system. The method for detecting angular deflection is to measure the linear displacement at a known radial distance using a linear variable differential transformer (LVDT). For the forces measured in this study, the linear movement at the end of the TSMB arm is on the order of a micrometer. Therefore, the error associated with the angular movement of the thrust stand arm is negligible. The motion of the TSMB is damped by a permanent magnet arrangement that uses eddy currents to provide a viscous force. The TSMB is calibrated using an electrostatic comb system described by Selden and Ketsdever [9].

For pulsed thruster systems, the TSMB is inverted with a horizontal axis of rotation. In this configuration, the TSMB can measure impulse and propellant mass loss simultaneously. To demonstrate the effectiveness of the TSMB, laser ablation events were investigated. Tests were configured using an 800-mJ-per-pulse Infinity Nd:YAG laser to ablate several material targets. Target materials were placed on the TSMB, located in a vacuum chamber capable of maintaining background pressures of $10^{-6}$ torr. The Infinity laser was configured to emit a wavelength of 532 nm at a repetition rate of 100 Hz. A shutter was situated in the path of the laser, and a pulse generator was used to trigger the shutter, resulting in an average of 35 shots arriving at the target. On the path to the target, the laser passed through a beam splitter, allowing the power of the laser to be monitored and the number of pulses per test to be counted. Testing was performed on several engineering surfaces, including machine-grade Teflon, Buna, and Viton. For these tests, the average number of shots on each site was held constant, whereas the energy of the laser was varied between 50 and 400 mJ IR. A calibration procedure using electrostatic combs [9] was conducted before the start of testing on each new target.

Upon completion of the tests, the data were analyzed to determine the impulse and mass loss of the material. This procedure required the data trace from the TSMB to undergo two different analyses. The first step was the determination of the mass lost during the ablation event. The analysis takes the average of the data points both before and after the ablation event. These averages are then used to determine the total stand deflection due to the steady-state mass lost from the target. The averages are also used to remove any electronic (thermal) drift in the LVDT. Because the total sampling time of an individual impulse event is relatively short (on the order of minutes), thermal drift is not significant, as shown in previous work [7,8]. The corresponding LVDT voltage change due to the propellant mass loss is shown in Fig. 6a. Using the steady-state calibration data from the electrostatic combs, the change in voltage can be directly correlated with a force associated with the change in target weight. The second step of the data analysis is to determine the impulse from the laser ablation event. This step analyzes the maximum deflection of the LVDT, which occurred between the first peak and first valley of the trace, as shown in Fig. 6b. Using pulsed-mode calibration data from the electrostatic combs, the maximum deflection can be directly correlated with an impulse.

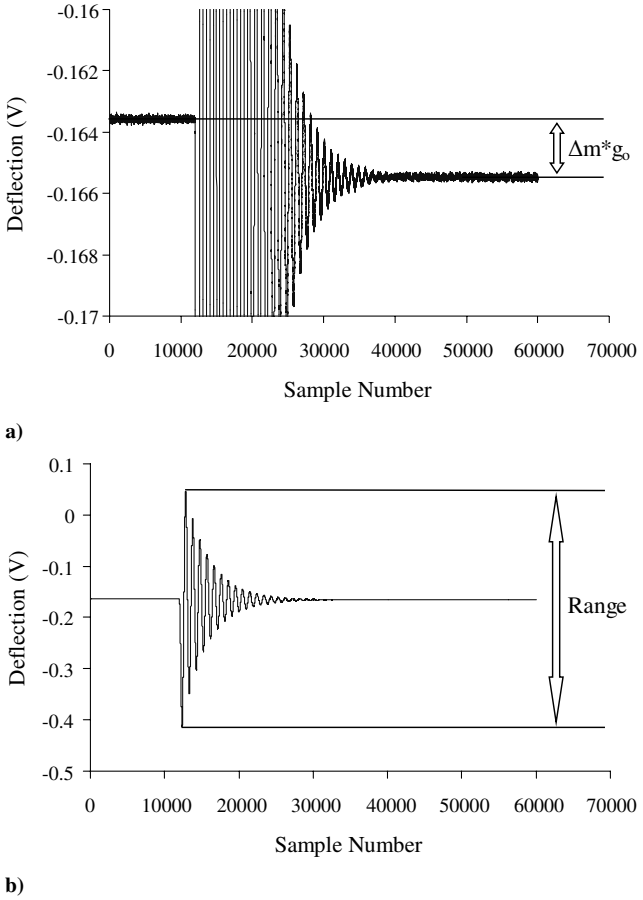


**Fig. 6 Sample trace from TSMB showing a) LVDT voltage change due to mass loss and b) the range.**

## Results and Discussion

The common measure of propulsive efficiency is the specific impulse. The specific impulse is a measure of the impulse per unit of expended propellant weight. From a propulsion-efficiency perspective, it is desirable to get the largest impulse for the lowest mass loss (i.e., high specific impulse). In its simplest form only the total impulse measurement and mass loss measurement are required to calculate the specific impulse. Figure 7 shows the impulse and corresponding ablative mass loss for a Buna target as a function of the total laser energy delivered to the target material. There is an increase in both impulse and mass loss as the laser energy increases, which leads to a general increase in the specific impulse shown in Fig. 8. The scatter in the data evident in Fig. 8 may come from a variety of sources. In the calibration process, the TSMB has repeatability of less than 1% (one sigma error). The scatter in Fig. 8 is much greater than 1%, indicating that the physical ablation process is most likely the

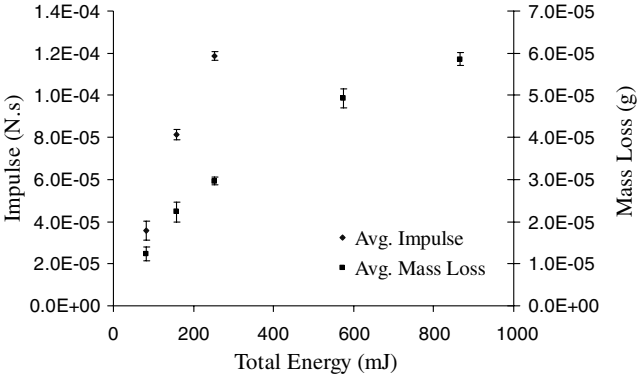


**Fig. 7 Impulse and mass loss for Buna target.**

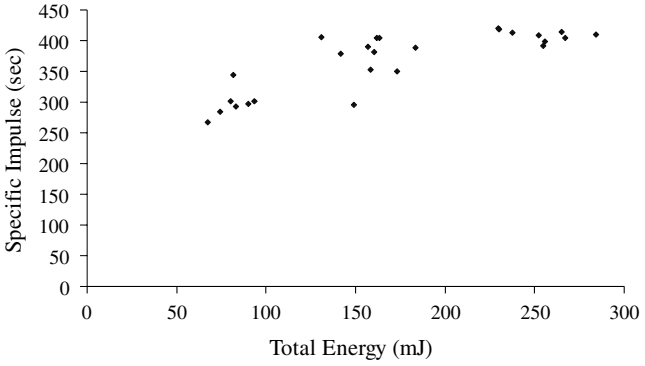


**Fig. 8 Specific impulse of Buna.**

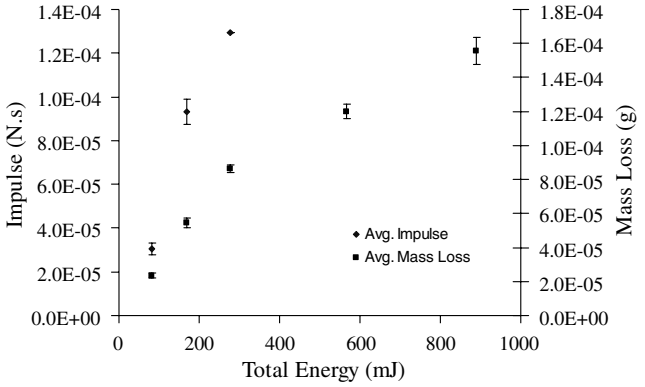


**Fig. 9 Impulse and mass loss for Viton.**

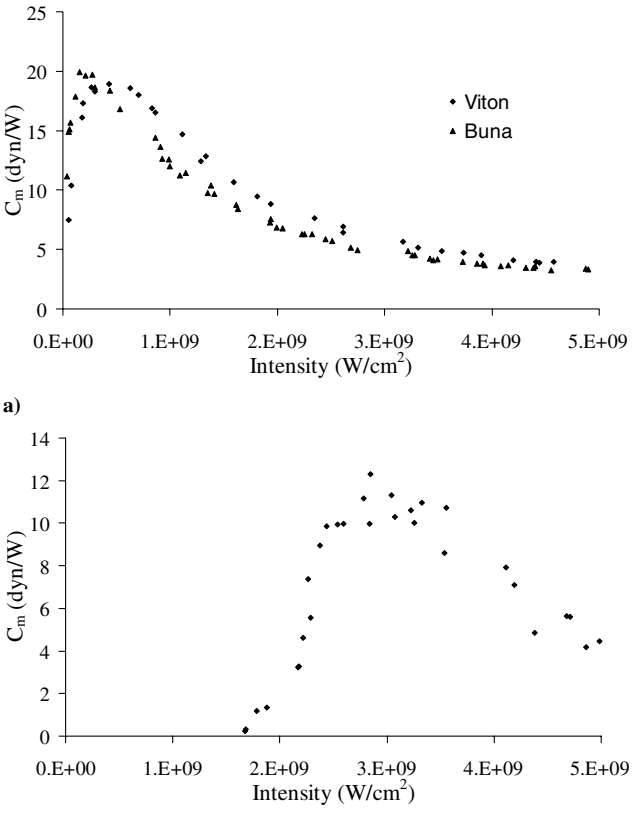


**Fig. 11 Coupling coefficients for a) mechanical grade Teflon and b) Viton and Buna.**

reason. Each data point represents a different test at a different target material location. Variations in laser output, surface roughness, and material impurities are the most likely causes of the scatter.

Figure 9 shows similar impulse and mass loss results for Viton. The specific impulse for these measurements is shown in Fig. 10. It is evident that the specific impulse increases with total laser energy up to about 175 mJ. At energies above 175 mJ the specific impulse tends to decrease. This trend can be explained by investigating the momentum coupling coefficient between the material and the incident laser beam. Phipps et al. [10] predict that the impulse efficiency, as measured by the momentum coupling coefficient, rapidly reaches a maximum once the ablation threshold is surpassed and then decreases with increasing laser intensity. The reduction in the efficiency can stem from several factors, including the shielding of the laser beam by ablating material. The coupling coefficients as a function of laser intensity are shown in Fig. 11a for Viton and Buna [11]. It should be noted that both materials have relatively low ablation thresholds and correspondingly high maximum coupling coefficients. Figure 11b shows the coupling coefficient for machine-grade Teflon. Note that the ablation threshold for Teflon is noticeably higher than for either Buna or Viton and the maximum coupling coefficient is lower.

Figure 12 shows impulse and mass loss for machine-grade Teflon with the corresponding specific impulse shown in Fig. 13. The specific impulse tends to decrease for total laser energies above about 300 mJ. The specific impulse for Teflon is generally lower than it is for either Buna or Viton, which correlates to its lower maximum coupling coefficient. The momentum coupling coefficient can be found from

$$C_m = \frac{I_{\text{tot}}}{E} = \frac{F}{P} \tag{12}$$

and the specific impulse can then be written as

$$I_{\text{sp}} = \frac{C_m Q^*}{g_o} \tag{13}$$

where $Q^* = E/\Delta m$. Therefore, both $C_m$ and $Q^*$ are dependent on the laser energy incident upon a particular material target. Figure 7 or

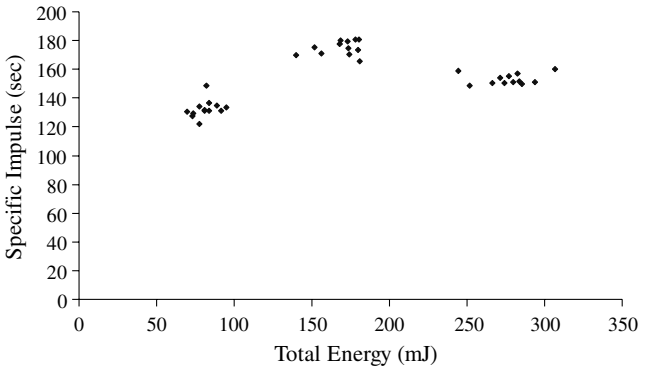


**Fig. 10 Specific impulse of Viton.**

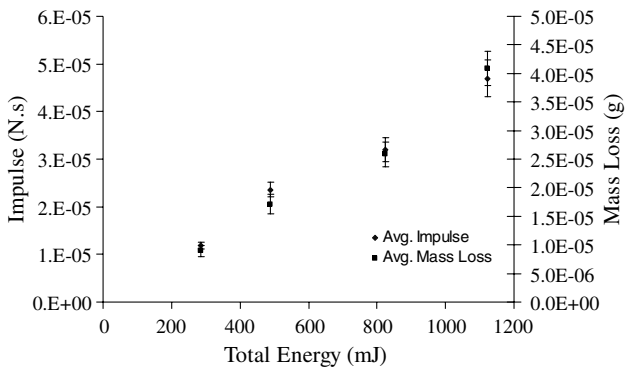


**Fig. 12 Impulse and mass loss for machine-grade Teflon.**

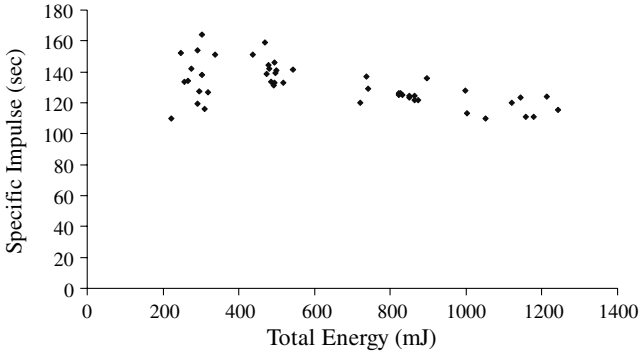


**Fig. 13 Specific impulse of machine-grade Teflon.**

Fig. 9 could be reformatted to show $C_m$ and $Q^*$ as a function of laser energy or total power. As can be seen, both the impulse $C_m$ and mass loss $Q^*$ are functions of the laser operating conditions, and thus $Q^*$ is not a constant. This implies that there is not a straightforward relationship between $I_{sp}$ and $C_m$. However, general trends in $I_{sp}$ can be inferred from Eq. (13). For a given $Q^*$, a larger $C_m$ implies a larger $I_{sp}$. Also, the $I_{sp}$ will be zero for laser energies below the ablation threshold at which $C_m = 0$. In general, these trends are verified by the data shown for the specific impulse. The data in Figs. 8, 10, and 13 show the ability of the TSMB to consistently measure the specific impulse from laser ablation events. In these cases, both mass loss and impulse were successfully extracted from a single TSMB trace.

## Conclusions

The TSMB has been used to consistently measure mass loss and impulse for laser ablation events. The ability to concurrently resolve impulse and mass loss from a single TSMB trace allows for the direct measurement of specific impulse. Although some scatter is visible in the data, there are multiple factors that could contribute to this scatter. For instance, the surface roughness of the spot being ablated could vary between test sites. The trends measured in the laser ablation specific impulse were consistent with the coupling coefficients for the various target materials. Buna exhibited the largest specific impulse for the incident laser energies investigated in this study. The TSMB showed its usefulness as a diagnostic tool for the direct measurement of specific impulse from laser ablation thrusters by demonstrating that specific impulses in the range of hundreds of seconds were achievable for laser ablation thrusters on engineering surfaces. However, the model results also indicate that the TSMB will be useful for other pulsed thruster systems. The major requirement of the thruster system is that the thruster firing time be no more than approximately one-quarter of the TSMB natural period for the inherent measurement error to remain below 0.5%. The natural period of the balance can be modified by changing either the associated spring constant or moment of inertia, allowing flexibility for a particular thruster system. The TSMB has shown its utility as a diagnostic tool for propulsion systems in which the measurement of mass flow is not straightforward. Mostly, these are solid propellant systems such as laser ablation thrusters, pulsed plasma thrusters, and hybrid thrusters.

## Acknowledgments

This work was supported by the U.S. Air Force Office of Scientific Research and the U.S. Air Force Research Laboratory (AFRL), Propulsion Directorate, Edwards Air Force Base, California. The authors wish to thank Jean-Luc Cambier (AFRL) for his support of the laser ablation measurements.

## References

[1] Sutton, G. P., and Biblarz, O., *Rocket Propulsion Elements*, 7th ed., Wiley-Interscience, New York, 2001.

[2] Fredrick, R. A., and Greiner, B. E., "Laboratory-Scale Hybrid Rocket Motor Uncertainty," *Journal of Propulsion and Power*, Vol. 12, No. 3, 1996, pp. 605–611. doi:10.2514/3.24076

[3] Lewis, D., Janson, S., Cohen, R., and Antonsson, E., "Digital Micro-Propulsion," *Sensors and Actuators A (Physical)*, Vol. 80, No. 2, 2000, pp. 143–154. doi:10.1016/S0924-4247(99)00260-5

[4] Burton, R. L., and Turchi, P. J., "Pulsed Plasma Thruster," *Journal of Propulsion and Power*, Vol. 14, No. 5, 1998, pp. 716–735.

[5] Hauer, M. R., "Laser Ablation of Polymers Studied by Time Resolved Methods," Ph.D. Dissertation, Swiss Federal Inst. of Technology, Zurich, 2004.

[6] Lin, J., Thompson, M. S., and Pakhomov, A. V.,"Ablative Laser Propulsion: Determination of Specific Impulse from Plasma Imaging," *High-Power Laser Ablation V*, Proceedings of SPIE, Vol. 5448, SPIE —The International Society for Optical Engineering, Bellingham, WA, 2004, pp. 465–476.

[7] D'Souza, B. C., and Ketsdever, A. D., "Investigation of Time-Dependent Forces on a Nano-Newton-Second Impulse Balance," *Review of Scientific Instruments*, Vol. 76, No. 1, 2005, Paper 015105. doi:10.1063/1.1834707

[8] Jamison, A., Ketsdever, A. D., and Muntz, E. P., "Gas Dynamic Calibration of a Nano-Newton Thrust Stand," *Review of Scientific Instruments*, Vol. 73, No. 10, 2002, pp. 3629–3637. doi:10.1063/1.1505096

[9] Selden, N., and Ketsdever, A. D., "Comparison of Force Balance Calibration Techniques for the Nano-Newton Range," *Review of Scientific Instruments*, Vol. 74, No. 12, 2003, pp. 5249–5254. doi:10.1063/1.1623628

[10] Phipps, C. R., Turner, T. P., Harrison, R. F., York, G. W., and Osbourne, W. Z., "Impulse Coupling to Targets in Vacuum by KrF, HF, and $CO_2$ Single-Pulse Lasers," *Journal of Applied Physics*, Vol. 64, No. 3, 1988, pp. 1083–1096. doi:10.1063/1.341867

[11] D'Souza, B. C., "Development of Impulse Measurement Techniques for the Investigation of Transient Forces Due to Laser-Induced Ablation," Ph.D. Dissertation, Univ. of Southern California, Dept. of Mechanical and Aerospace Engineering, Los Angeles, 2006.

C. Segal
*Associate Editor*